Water Research X 1 (2018) 100008

Contents lists available at ScienceDirect

Water Research X

journal homepage: https://www.journals.elsevier.com/water-research-x

Ion selectivity in capacitive deionization with functionalized electrode: Theory and experimental validation

Diego I. Oyarzun [a], Ali Hemmatifar [a], James W. Palko [b], Michael Stadermann [c], Juan G. Santiago [a, *]

[a] Department of Mechanical Engineering, Stanford University Stanford, CA 94305, USA
[b] Department of Mechanical Engineering, University of California, Merced, CA 95343, USA
[c] Lawrence Livermore National Laboratory, 7000 East Avenue, Livermore, CA 94550, USA

ARTICLE INFO

Article history:
Received 25 May 2018
Received in revised form
30 October 2018
Accepted 31 October 2018
Available online 5 November 2018

Keywords:
Ion selectivity
Capacitive deionization
Nitrate
Surface charge
Surfactant treatment

ABSTRACT

Capacitive deionization (CDI) is a promising technique for salt removal and may have potential for highly selective removal of ion species. In this work, we take advantage of functional groups usually used with ionic exchange resins and apply these to CDI. To this end, we functionalize activated carbon with a quaternary amines surfactant and use this surface to selectively and passively (no applied field) trap nitrate ions. We then set the cell voltage to a constant value to regenerate these electrodes, resulting in an inverted capacitive deionization (i-CDI) operation. Unlike resins, we avoid use of concentrated chemicals for regeneration. We measure the selectivity of nitrate versus chloride ions as a function of regeneration voltage and initial chloride concentration. We experimentally demonstrate up to about 6.5-fold (observable) selectivity in a cycle with a regeneration voltage of 0.4 V. We also demonstrate a novel multi-pass, air-flush i-CDI operation to selectively enrich nitrate with high water recovery. We further present a dynamic, multi-species electrosorption and equilibrium solution-to-surface chemical reaction model and validate the model with detailed measurements. Our i-CDI system exhibits higher nitrate selectivity at lower voltages; making it possible to reduce $NaNO_3$ concentrations from ~170 ppm to below the limit of maximum allowed values for nitrate in drinking water of about 50 ppm $NaNO_3$.

1. Introduction

Lack of accessible clean water is a growing concern worldwide. Selective ion removal can play a crucial role for the extraction of ionic contaminants and/or rare metal ions from aqueous solutions and reduce the cost of treating water. Nitrate is an example of a common potentially toxic anion in brackish water (Bouchard et al., 1992; Inoue-Choi et al., 2014; Jones et al., 2016). Thus, highly selective desalination is relevant for point-of-use water purification systems and industrial applications. Widely used techniques for removal of organic and inorganic contaminants include reverse osmosis (RO) (Richards et al., 2011; Xie et al., 2012), forward osmosis (FO) (Kumar and Pal, 2015), electrodialysis (ED), nanofiltration (NF) (Ghaemi et al., 2018), and ionic exchange resins (Samatya et al., 2006; Xu et al., 2012). Membrane technologies such as RO or FO are predominantly used for sea water desalination and often have significantly high salt rejection (98% or higher (Chekli et al., 2016; Jamaly et al., 2014; Subramani and Jacangelo, 2015; Zhao et al., 2017)). However, such technologies are not readily optimized for treatment of lower salinity streams such as brackish water or in applications targeted towards removal of specific ions in the solution (Werber et al., 2016). Ion exchange resins are one alternative method. Charged groups on the surface of the resins are initially electrostatically shielded by low-affinity ions (e.g., Cl^-), but can then adsorb higher affinity ions (e.g., NO_3^-) via ion exchange. This affinity is currently not sufficiently well understood for first-principles predictions of quantitative affinity, but adsorption kinetics are known to be influenced by ion size and electronic structure, and the associated interaction with ionic surface groups (Harland, 1994). Although use of ion exchange resins is promising for selective ion removal, it suffers from significant drawbacks. Most notably are the requirement for high concentration chemicals used during regeneration, and the disposal of these chemicals after regeneration.

Capacitive deionization (CDI) and sub-categories such as

* Corresponding author.
E-mail address: juan.santiago@stanford.edu (J.G. Santiago).

https://doi.org/10.1016/j.wroa.2018.100008

inverted capacitive deionization (i-CDI) and membrane capacitive deionization (MCDI) are electrochemical techniques which use electrosorption to adsorb/desorb ions onto/from high surface area electrodes. Specifically, in CDI a potential is applied to electrostatically adsorb ions; while in i-CDI native surface charges on porous electrodes are used to adsorb ions (e.g. with no applied potential), and an external potential is then applied to regenerate the electrode(s). CDI and i-CDI have been mainly focused on reduction of salinity, but recent efforts have explored removal of specific ionic contaminants from water (Farmer et al., 1996; Oren, 2008; Seo et al., 2010). CDI and i-CDI offer advantages over ion exchange resins in that they require no highly concentrated chemicals for regeneration. In i-CDI, an electric field is applied to regenerate the cell, and this also implies the possibility of energy recovery during the adsorption step (Gao et al., 2015).

Selective ion removal has been an active area of research in CDI community in recent years. The selectivity of adsorption has been attributed mainly to ion valence and steric effects (Han et al., 2014; Hou et al., 2008; Hou and Huang, 2013; Li et al., 2016; Seo et al., 2010), and the interaction between nanoporous size and hydrated radius also seems to play a significant role (Han et al., 2014; Hou et al., 2008; Hou and Huang, 2013; Li et al., 2016; Nie et al., 2011). Selectivity has been demonstrated experimentally for lithium (Lee et al., 2017; Siekierka et al., 2017a,b; Siekierka and Bryjak, 2017), nitrate (Tang et al., 2016a, 2016b), and fluoride removal (Lado et al., 2017; Tang et al., 2015; Yeo and Choi, 2013). However, these studies relied on the intrinsic selectivity of pristine activated carbon surfaces (Han et al., 2014; Hou and Huang, 2013; Seo et al., 2010). Other studies (Kim et al., 2013; Kim and Choi, 2012) coated the surface of the activated carbon electrodes with an anion-exchange resin which then served as an ion selective barrier (this is discussed further below).

In previous work, we used nitrate selective moieties of a type shown to be effective for nitrate selective extraction using ion exchange resin absorbents (Oyarzun et al., 2018; Palko et al., 2017; Wheaton and Bauman, 1951). The physical mechanism for adsorption of these moieties relies on the ionic exchange of the selective surface group, a quaternary ammonium. Such surface groups are initially weakly bound to a low-affinity counter charged ion (i.e. chloride). Upon exposure to a solution containing a high-affinity ion (i.e. nitrate), there is an exchange between the low-affinity chloride with the high-affinity nitrate. The system of Palko et al. (2017) was very limited in practicality and energy efficiency since only a single electrode was functionalized, and the counter electrode sustained a Faradaic reaction to drive overall current in the cell. This significant drawback was addressed by Oyarzun et al. (2018) who functionalized one electrode with cetyltrimethylammonium bromide (CTAB) and the second with sodium dodecylbenzenesulfonate (SDBS), hence a more complete i-CDI cell. Despite this, the latter study was also limited in several ways. First, the measurements quantifying adsorption and desorption were for pure sodium nitrate solutions, and so no selectivity was demonstrated. Second, the study presented no theory capable of predicting the dynamic steady state of the multi-species adsorption and desorption dynamics. Third, the study provided no way to continuously enrich selectively adsorbed nitrate in multiple cycles (or air flushing of any kind). These three shortcomings are addressed in the current work.

We note that the current functionalization differs significantly from the work of (Kim et al., 2013; Kim and Choi, 2012) in that we here use no anion-exchange barrier or membrane (or absorbance medium) of any kind to treat the activated carbon. Instead, we adsorb (to the surface of) CTAB and SDBS to the electrodes to achieve a selective adsorption function. In our approach, ions neither cross a membrane barrier nor are absorbed into any medium, but instead are adsorbed directly to a treated surface. As mentioned above, we also address shortcomings of the work of Palko et al. (2017) and Oyarzun et al. (2018) by providing a theoretical framework to model the competition of adsorption (desorption) of multispecies, by quantifying the simultaneous (and competitive) adsorption of chloride versus nitrate ions, and by exploring a novel recirculation method to selectively preconcentrate species. To this end, we explore the competition between the low affinity ion (chloride) and the high affinity ion (nitrate) onto the CTAB-functionalized electrode. CTAB has been used for the selective removal of nitrate over chloride in (permeable) ion exchange membranes (Barron and Fritz, 1984) but not in i-CDI. We study experimentally the effect of regeneration voltage and inlet concentrations on ion removal using species-specific ion chromatography (IC) quantification of the outlet stream species. As we shall see, we achieve high values of selectivity and demonstrate an dynamic model useful to selectively remove ions and reduce ion concentrations below regulations limits (World Health Organization, 2011).

We also present a model to guide our design and optimize our system. A number of models have been presented to explain selectivity, and these have focused on either ion size effects (compared to pore structure) (Suss, 2017) or on ion valence and its effect on electrostatics (Zhao et al., 2012). The latter models lack a detailed treatment (including competitive selectivity) of the differing affinity of surface groups of the activated carbon surface. We here expand on the steady-state model presented by Hemmatifar et al. (2017) to model and study the effect of surface treatment on ion adsorption. Additionally, we perform experiments and develop time-dependent predictions of the dynamics of ion-selective desalination. Our model combines a Donnan treatment for electric double layers and electrosorption Langmuir-type equilibria. Our electrostatics treatment includes chemical surface charge for functionalized activated carbon which we incorporate as a first order, species-specific equilibrium reaction model for adsorption. We model transport through the cell using a well-mixed reactor model.

2. Theory

2.1. Equilibrium model for ion selectivity

We recently developed a weak electrolyte equilibria model for activated carbons with charged functional groups and showed effect of pH on carbon's surface charge and its ability to adsorb in the absence of applied electric fields (Hemmatifar et al., 2017). This is in contrast with contributions where chemical adsorption has been modeled using a constant surface charge (Biesheuvel et al., 2015; Dykstra et al., 2017; He et al., 2018; Mubita et al., 2018). We here show a modification of such a model and demonstrate (competitive) adsorption selectivity of ions onto the surfactant-treated carbon surfaces. We make the following assumptions: (1) moderate pH range (4–10) (Persat et al., 2009) such that salt concentration is considerably larger than that of hydronium and hydroxide ions and (2) surfactant functional groups dominate the native, weak-electrolyte surface charge groups associated with the bare carbon (Hemmatifar et al., 2017). The latter assumption implies that the chemical surface charge on the electrode is primarily due to strong electrolyte behavior of the surfactants. In Section 4.2, we show validity of these two assumptions for the current study. A more general formulation of the model which includes pH effects is presented in Section S1 of the Supplementary Information.

Next, we model the intrinsic affinity of anionic species (i.e. chloride and nitrate ions) to CTAB-treated activated carbon electrode (CTA-AC) with equilibrium reactions of the form

$$CTACl \overset{K_{Cl}}{\rightleftharpoons} CTA^+ + Cl^- \quad (1)$$

$$CTANO_3 \overset{K_{NO_3}}{\rightleftharpoons} CTA^+ + NO_3^- \quad (2)$$

and intrinsic affinity of cationic species (i.e. sodium ions) to SDBS-treated electrode (DBS-AC) as

$$DBSNa \overset{K_{Na}}{\rightleftharpoons} DBS^- + Na^+ \quad (3)$$

where K_{Cl}, K_{NO_3}, and K_{Na} are equilibrium constants for adsorption of chloride, nitrate, and sodium ions, respectively, and can be written as

$$K_{Cl} = c_{CTA^+} c_{m,Cl^-,A}/c_{CTACl} \quad (4)$$

$$K_{NO_3} = c_{CTA^+} c_{m,NO_3^-,A}/c_{CTANO_3} \quad (5)$$

$$K_{Na} = c_{DBS^-} c_{m,Na^+,C}/c_{DBSNa}. \quad (6)$$

Here, c_{CTA^+}, c_{CTACl}, c_{CTANO_3}, c_{DBS^+}, and c_{DBSNa} are the concentrations of the respective surfactant species (in units of moles per micropore volume), and $c_{m,Cl^-,A}$, $c_{m,NO_3^-,A}$, and $c_{m,Na^+,C}$ are micropore concentrations of chloride and nitrate ions in CTA-AC and sodium ions in DBS-AC, respectively. The subscript m denotes micropore and A and C denote active and counter electrode (the micropore vs. macropore treatment of electrodes is discussed at the start of the next section). Species conservation can be written in terms of the analytical concentrations of surfactant groups on CTA-AC electrode ($c_{CTA,0}$) and DBS-AC electrode ($c_{DBS,0}$) as

$$c_{CTA,0} = N_{CTA,0}/v_m = c_{CTA^+} + c_{CTACl} + c_{CTANO_3} \quad (7)$$

$$c_{DBS,0} = N_{DBS,0}/v_m = c_{DBS^-} + c_{DBSNa} \quad (8)$$

where $N_{CTA,0}$ and $N_{DBS,0}$ are net amount (moles) of surfactant on CTA-AC and DBS-AC electrodes, and v_m is the micropore volume. Note, CTA-AC and DBS-AC electrodes have positive and negative chemical charge, respectively. The chemical charge density of surfactants on the electrodes can then be written as

$$\sigma_{chem,A} = Fc_{CTA^+} = Fc_{CTA,0}\left(1 + \frac{c_{m,Cl^-}}{K_{Cl}} + \frac{c_{m,NO_3^-}}{K_{NO_3}}\right)^{-1} \quad (9)$$

$$\sigma_{chem,C} = -Fc_{DBS^-} = -Fc_{DBS,0}\left(1 + \frac{c_{m,Na^+}}{K_{Na}}\right)^{-1} \quad (10)$$

where F is Faraday's constant.

2.2. Electric double-layer model

We use a Donnan model for description of electronic double layer (EDL), where the micropore EDLs are treated as strongly overlapping (Biesheuvel et al., 2011; Hemmatifar et al., 2015). A detailed description of this model is given in our recent work (Hemmatifar et al., 2017); so we here summarize the important results. Concentration of ions within the micropores can be related to that of macropores (outside EDLs) with a Boltzmann distribution of the form

$$c_{m,i,j} = c_i\, exp(-z_i \Delta\phi_{D,j}/V_T) \text{ with } i = Cl^-, NO_3^-, Na^+ \text{ and } j = A, C \quad (11)$$

where $c_{m,i,j}$ is micropore concentration of ion i (chloride, nitrate, or sodium ions) in the electrode j (A for anode and C for cathode), c_i and z_i are the corresponding macropore concentration and valence of ion i, and $\Delta\phi_{D,j}$ is Donnan potential in the electrode j. The chemical, ionic, and electronic charge density add up to zero in each electrode (i.e. net neutral charge compensation) as in

$$\sigma_{chem,j} + \sigma_{ionic,j} + \sigma_{elec,j} = 0 \text{ with } j = A, C \quad (12)$$

where $\sigma_{ionic,j} = F\sum z_i c_{m,i,j}$ is the ionic and $\sigma_{elec,j} = C_m \Delta\phi_{m,j}$ is the electronic charge density of electrode j, respectively (C_m and $\Delta\phi_{m,j}$ being volumetric capacitance and micropore potential drop). We also assume that the electronic charges applied to the electrodes are antisymmetric, hence we write

$$v_{m,A}\sigma_{elec,A} + v_{m,C}\sigma_{elec,C} = 0, \quad (13)$$

where $v_{m,A}$ and $v_{m,C}$ are respectively the micropore volumes for the anode and cathode respectively, and we assume $v_{m,A} = v_{m,C}$.

2.3. Mass transport equations

We here assume an open-loop i-CDI system with continuous flow from reservoir to the cell with constant feed concentration. We assume a well-mixed reactor model with first-order kinetics for functional groups on CTA-AC and DBS-AC electrode (as described in Section 4.1). For our multi-species system, the mass transport equations for chloride and nitrate ions can thus be written as

$$v_{cell}\frac{dc_{Cl^-}}{dt} = Q\left(c_{Cl^-,0} - c_{Cl^-}\right) - v_m\frac{d}{dt}\left(c_{m,Cl^-,A} + c_{CTACl} + c_{m,Cl^-,C}\right) \quad (14)$$

$$v_{cell}\frac{dc_{NO_3^-}}{dt} = Q\left(c_{NO_3^-,0} - c_{NO_3^-}\right) - v_m\frac{d}{dt}\left(c_{m,NO_3^-,A} + c_{CTANO_3} + c_{m,NO_3^-,C}\right) \quad (15)$$

where c_{Cl^-} and $c_{NO_3^-}$ are the effluent concentrations of chloride and nitrate ions, v_{cell} is cell volume, and Q is the flow rate. For the third species (here, sodium) we invoke electroneutrality condition and relate concentration of Na^+ to that of Cl^- and NO_3^- as

$$c_{Na^+} = c_{Cl^-} + c_{NO_3^-} \quad (16)$$

2.4. External circuit

We now couple mass transport equations above with the external circuit. First, the external applied voltage V_{ext} can be related to anode and cathode potentials (V_A and V_C) as

$$V_{ext}(t) = I_{ext}R_s + (V_A - V_C) \quad (17)$$

with $V_A - V_C = (\Delta\phi_{D,A} + \Delta\phi_{m,A}) - (\Delta\phi_{D,C} + \Delta\phi_{m,C})$. Here, I_{ext} is the external current measured with a sourcemeter, and R_s is the net series resistance in the system (including resistance of wires, electrode-current collector contact resistance, and resistance of solution in spacers). For simplicity, we model the resistance R_s as sum of electronic resistance $R_{s,\,elec}$ and ionic resistance $R_{s,\,ionic}$. We model the latter as

$$R_{s,ionic} = \frac{\lambda_0}{\lambda_{Na} c_{Na} + \lambda_{Cl} c_{Cl} + \lambda_{NO_3} c_{NO_3}} \tag{18}$$

where λ_0, λ_{Na}, λ_{Cl}, and λ_{NO_3} are constants that relate ionic concentrations to ionic resistance of the cell. Finally, the applied voltage V to the two-electrode i-CDI system can be written as

$$V_{cell} = I_{ext} R_s + (\Delta\phi_{D,A} + \Delta\phi_{m,A}) - (\Delta\phi_{D,C} + \Delta\phi_{m,C}) \tag{19}$$

2.5. Intrinsic and cycle selectivity

In the ion-exchange resin literature, the selectivity of an ion relative to another is often characterized using a selectivity coefficient defined as the ratio of enrichment factors for the two ions of interest, or equivalently, ratio of equilibrium constants. By *enrichment factor*, we mean ratio of concentration on the exchanger (stationary phase) over concentration in the external solution (mobile phase) (Hasnat and Juvekar, 1996; Helfferich, 1962). This parameter is measurable only in controlled and near-equilibrium conditions, and so we hereafter refer to this coefficient as the *intrinsic* selectivity coefficient. For example, this intrinsic parameter is strictly only valid and observable in the absence of an applied voltage to the cell. As an example, the intrinsic selectivity coefficient of nitrate with respect to chloride on CTAB-treated electrode can be written as

$$k_{int} = \frac{K_{NO_3}}{K_{Cl}} = \frac{c_{CTANO_3}/c_{NO_3^-}}{c_{CTACl}/c_{Cl^-}} \tag{20}$$

where c_{Cl^-} and $c_{NO_3^-}$ are concentrations in external solution in the case of no applied voltage (note, in general, this is different from zero voltage). The external voltage can alter this intrinsic selectivity towards higher or lower selectivity coefficient values. The set of equations in Sections 2.1 to 2.3 can be solved to calculate the *modified* selectivity coefficient (due to applied voltage), for which we here propose the following definition:

$$\tilde{k}_{int} = \frac{\left(c_{CTANO_3} + \Delta c_{NO_3^-}\right)/c_{NO_3^-}}{(c_{CTACl} + \Delta c_{Cl^-})/c_{Cl^-}} \tag{21}$$

or, equivalently, using mass conservation equations (15) and (16), as

$$\tilde{k}_{int} = \frac{\left(c_{NO_3^-,0} - c_{NO_3^-}\right)/c_{NO_3^-}}{\left(c_{Cl^-,0} - c_{Cl^-}\right)/c_{Cl^-}} \tag{22}$$

where $\Delta c_{NO_3^-}$ and Δc_{Cl^-} are excess micropore concentrations (increase in concentrations with respect to external solution) due to applied voltage and can be written as $\Delta c_i = c_{m,i,A} + c_{m,i,C} - 2c_i$ (for $i = Cl^-, NO_3^-$). Note that in the absence of external voltage, micropore and external solution concentrations are equal (i.e. $c_{m,i,j} = c_i$ for $i = Cl^-, NO_3^-$ and $j = A, C$). So, $\Delta c_i = 0$ and k_{int} is recovered.

We note that intrinsic selectivity coefficients (k_{int} and $\tilde{k}_{int}$) solely quantify preferential *adsorption* by chemical affinity. In CDI applications, however, the observable (in effluent) selective adsorption of one species versus others is determined by the dynamics of the coupled effects of this chemical affinity with electrosorption and mass transport. For example, CDI requires a regeneration (or desorption) step for cyclic operation, so that the achievable selectivity of both the adsorption and regeneration steps is influenced by the operational parameters of the CDI cell. In this work, we chose an operation scheme wherein surfactant-treated electrodes is used for selective adsorption of nitrate ions and this is then followed by a non-selective regeneration step. To quantify the preference of the CDI cell for nitrate ions in the voltage window V_{reg} (regeneration voltage) to V_{ads} (adsorption voltage), we define the new parameter we term the *cycle* selectivity coefficient k_{cycle}. For a closed-loop system, we define cycle selectivity coefficient as

$$k_{cylce} = \frac{\left[c_{NO_3^-}(V_{reg}) - c_{NO_3^-}(V_{ads})\right]/c_{NO_3^-,0}}{\left[c_{Cl^-}(V_{reg}) - c_{Cl^-}(V_{ads})\right]/c_{Cl^-,0}} \tag{23}$$

where numerator is relative change in concentration of nitrate in the external solution measured at the end of adsorption and regeneration steps. A brief analytical development of this expression is given in the SI. Note the denominator is the relative change for chloride ions. For open-loop systems, cycle selectivity coefficient can be calculated as

$$k_{cylce} = \frac{c_{Cl^-,0}}{c_{NO_3^-,0}} \frac{\int_0^{t_{ads}} \left(c_{NO_3^-,0} - c_{NO_3^-}(t)\right)\, dt}{\int_0^{t_{ads}} \left(c_{Cl^-,0} - c_{Cl^-}(t)\right)\, dt} \tag{24}$$

where $c_{NO_3^-}(t)$ and $c_{Cl^-}(t)$ are time-varying effluent concentration of nitrate and chloride, and t_{ads} is duration of adsorption step. Note that k_{cycle} can attain values very different (and significantly larger) than the intrinsic selectivity. For example, we will show in Section 4.2 that, for small voltage window, the equilibrium concentration of chloride in the external solution in adsorption step is very close to that of the regeneration step. This results in very large cycle selectivity but, as we shall see, this is at the cost of low salt adsorption capacity.

3. Materials and methods

3.1. Materials

We used commercially available activated carbon electrodes (Material Methods LLC., PACMM™ 203, Irvine, CA) and modified the surface charge of the activated carbon with anionic and cationic surfactants. Half of the pristine electrodes were functionalized with cetrimonium bromide (CTAB, $CH_3(CH_2)_{15}N(CH_3)_3Br$) cationic surfactant in order to enhance their anion adsorption capacity. The electrodes were soaked in 500 mL solution of 10 mM CTAB for 12 h, thoroughly rinsed with deionized (DI) water, and dried. We refer to this CTAB-treated activated carbon as CTA-AC from this point forward. The rest of the pristine electrodes were functionalized with sodium dodecyl benzene sulfonate (SDBS, $CH_3(CH_2)_{11}C_6H_4SO_3Na$) anionic surfactant to increase their cation adsorption capacity. Similarly, the electrodes were soaked in 500 mL of 10 mM SDBS solution for 12 h, rinsed with deionized (DI) water, and dried. We refer to SDBS-treated activated carbon as DBS-AC. The uptake of CTAB and SDBS by electrodes was approximately 446 and 489 mg (1.2 and 1.4 mmol) per g of electrodes measured by a total organic carbon analyzer (TOC-L autoanalyzer, Shimadzu, Kyoto, Japan).

3.2. Experimental setup

3.2.1. Intrinsic selectivity experiment

To calculate the intrinsic selectivity of the CTA-AC electrode for nitrate with respect to chloride, we performed the following adsorption equilibrium experiment. First, a sample of CTA-AC electrode was soaked in 150 mM NaCl for 24 h in order for Cl^- to replace Br^- that was originally on the electrode surface. The

process was repeated for a second time to exchange as much Br^- as possible with Cl^-. The total of exchanged bromide was 1.14 mmol per g of electrodes, which is ~95% of the initial CTAB uptake. Activated carbon electrodes were then washed with DI water and dried. Next, eight containers were filled with 24 ml of sodium nitrate solution with concentrations between 0.3 and 3 mM, and 50 mg of activated carbon was added to each container. The containers were sealed and gently agitated for 24 h, and the equilibrium concentration of nitrate and chloride was measured with IC.

3.2.2. i-CDI experiments

Fig. 1 shows the schematic of the i- CDI cell. Our i-CDI cell utilizes a radial inflow geometry wherein feed solution is injected into the system from the periphery of the stack of circular electrodes. The solution then flows radially inward between the electrode layers (through separators) and electrosorption or desorption occurs. The desalted (brine) solution then exits the system from the center of the porous electrode stack in a direction normal to the planes of the electrodes. See Hemmatifar et al. (2017), Oyarzun et al. (2018) and Palko et al. (2017) for descriptions of similar CDI cell architectures. We fabricated a flow-between i-CDI cell using a single pair of surfactant-treated electrodes with 3.5 cm diameter, ~300 μm thickness, and a total dry mass of 0.28 g. We used 50 μm thick titanium sheets as current collectors and a 300 μm thick woven plastic mesh (McMaster-Carr, Los Angeles, CA) as a spacer between the electrodes. Our i-CDI experimental setup consisted of the i-CDI cell, a 3 L reservoir, a sourcemeter (Keithley 2400, Cleveland, OH), and a peristaltic pump (Watson Marlow 120U/DV, Falmouth, Cornwall, UK). To exchange the bromide initially on CTA-AC electrode, we applied 0 V to the cell and maintained a continuous 0.23 ml min^{-1} flow of 2 mM $NaNO_3$ and 2 mM NaCl for 12 h. We then applied voltages of 0.4, 0.6, 0.8, 1, and 1.2 V for cell regeneration and 0 V (short circuit) for ion adsorption. In a separate set of experiments, we fixed the regeneration voltage and used different nitrate to chloride inlet concentrations. To this end, we applied 1 V in regeneration and 0 V in adsorption steps with a feed solution of 2 mM $NaNO_3$ mixed with 2, 4, or 8 mM NaCl. The duration of each regeneration or adsorption step in all experiments

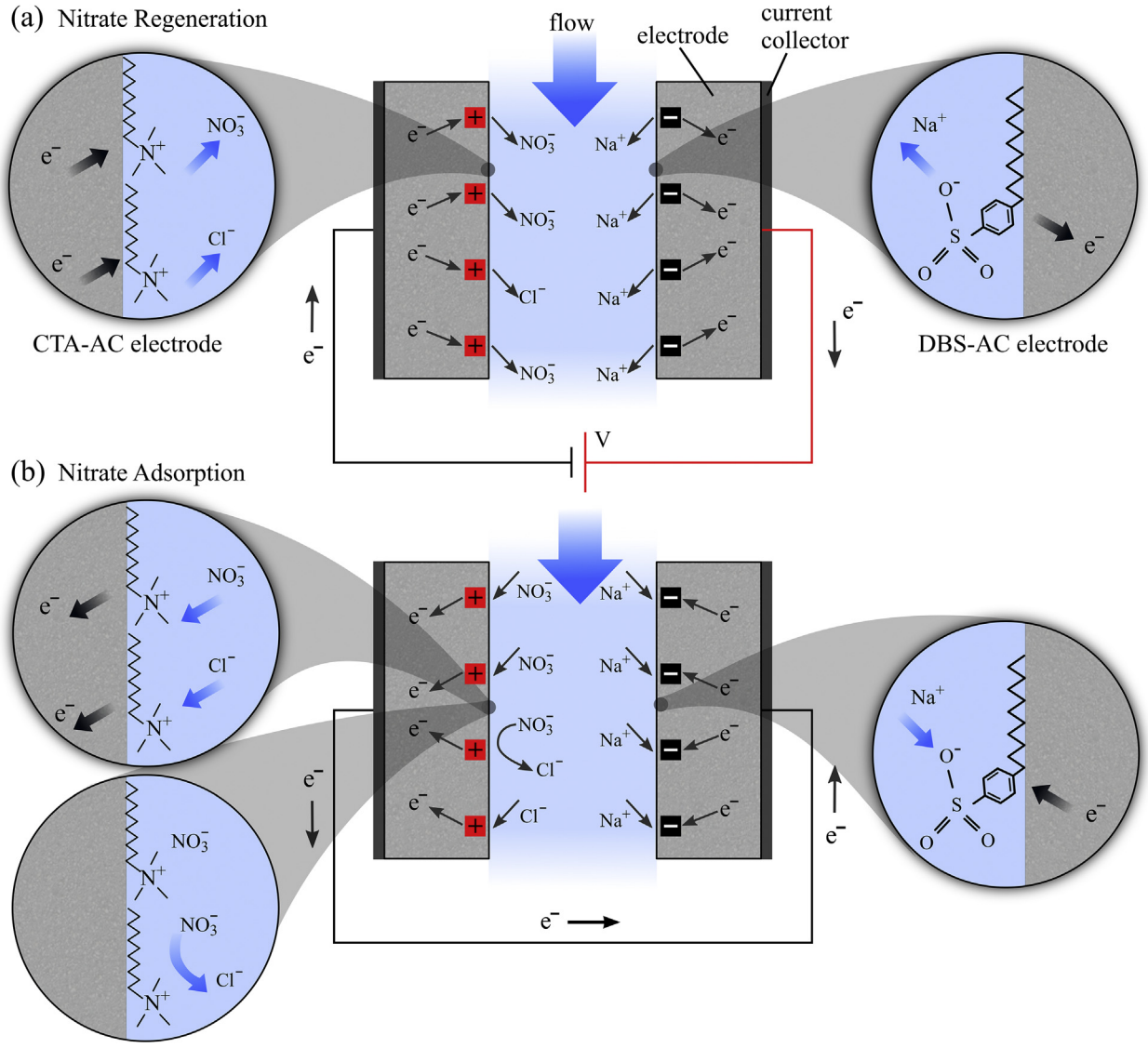

Fig. 1. Schematic of the i-CDI cell used in this study. One electrode (labeled CTA-AC) is treated with CTAB and a counter electrode (DBS-AC) is treated with SDBS. (a) Schematic of the regeneration step at constant voltage of the i-CDI cell. The applied bias forces electrons to migrate from DBS-AC to CTA-AC. Electrons driven toward CTA-AC repel Cl- and NO3- ions, while holes driven toward DBS-AC repel Na + ions. This process leaves an available surface charge in both electrodes (DBS-AC to CTA-AC). (b) Schematic of a simple short-circuit adsorption process. Na^+, Cl^-, and NO_3^- ions are adsorbed, forcing migration of electrons from CTA-AC to DBS-AC.

was 2 h. We collected effluent in aliquots accumulated over 10 min intervals and saved into separate containers using a fraction collector (Model 2128, Bio-Rad, CA). The ionic content of each sample was then measured using ion chromatography (DIONEX DX 500, DIONEX, CA) at the Stanford ICP-MS/TIMS Facility.

3.2.3. Up-concentration experiment

To demonstrate ion selective capacitive desalination, we fabricated a second, higher-capacity cell. This second cell was similar to that in Section 3.2.2 but featured three pairs of electrodes (three CTA-AC and three DBS-AC electrodes) with a total dry mass of 0.84 g. We use this cell to demonstrate and study a multi-pass, air-flush mode which we term "up-concentration" operation of our CTA-AC/DBS-AC system.

The up-concentration experiments were as follows. First, in the adsorption step, we fed a solution of 2 mM $NaNO_3$ and 2 mM NaCl at a 4 ml min^{-1} flow rate for 4 h and applied 0 V to the cell. A single-pass flow was used in this adsorption step, i.e. the solution passed through the cell once, and effluent was collected in a reservoir. After the adsorption step the cell was emptied of solution by pumping air into the system, while a voltage of 0 V was applied to the cell. Next, we performed a closed-loop circulation step by connecting the cell to a second reservoir, which we herein call brine reservoir (flow at 8 mL min^{-1} from the brine reservoir to the cell and back to the brine reservoir). This brine reservoir was initially filled with 154 mL of DI water. During regeneration, a voltage of 1 V was applied to the cell (negative lead to CTA-AC and positive lead to DBS-AC electrode) for 4 h to desorb the nitrate and chloride ions into the brine reservoir. To minimize cross-contamination, the solution in the cell and tubing was then emptied to the brine reservoir by flowing air into the system. At this point, we collected an 0.4 mL sample from the reservoir for the IC measurement. We repeated this process eight times and measured the nitrate and chloride content of the brine reservoir using IC. We show the results of this selective up-concentration experiment in Section 4.4.

4. Results and discussion

4.1. Quantification of intrinsic selectivity

As described in Section 3.2.1, we exchanged bromide initially on a sample of CTA-AC electrode with chloride. We then placed 50 mg pieces of treated electrodes into 8 containers filled with 24 mL $NaNO_3$ of various concentrations (0.3–3 mM). Nitrate and chloride content of the solutions was then measured with IC after 24 h equilibration time. Fig. 2 shows adsorption equilibrium of nitrate and chloride in the micropores (c_{CTANO_3}/c_{CTACl}) on the ordinate versus that of nitrate and chloride in the solution phase ($c_{NO_3^-}/c_{Cl^-}$) on the abscissa. Final concentrations of nitrate and chloride in the solution phase ($c_{NO_3^-}$ and c_{Cl^-}) were directly and independently measured using IC. Micropore concentration of nitrate and chloride was calculated indirectly using the following relation.

$$\frac{c_{CTANO_3}}{c_{CTACl}} = \frac{n_{NO_3^-} - v_{sol}\, c_{NO_3^-}}{n_{Br^-} - v_{sol}\, c_{Cl^-}}. \tag{25}$$

where $n_{NO_3^-}$ is amount (moles) of nitrate ions added to the solution and n_{Br^-} is amount (moles) of released bromide initially bound to CTA-AC electrode. The latter is approximately equal to amount of exchanged chloride, we measured this quantity in Section 3.2.1. In Fig. 2, markers show experimental results and solid line is linear regression based on the mean squared error ($R^2 = 0.9952$). Based on slope of regression line, the intrinsic selectivity coefficient of nitrate with respect to chloride is approximately 7.7. We will use this measured intrinsic selectivity coefficient in the model as $k_{int} = K_{Cl}/K_{NO_3} \approx 7.7$.

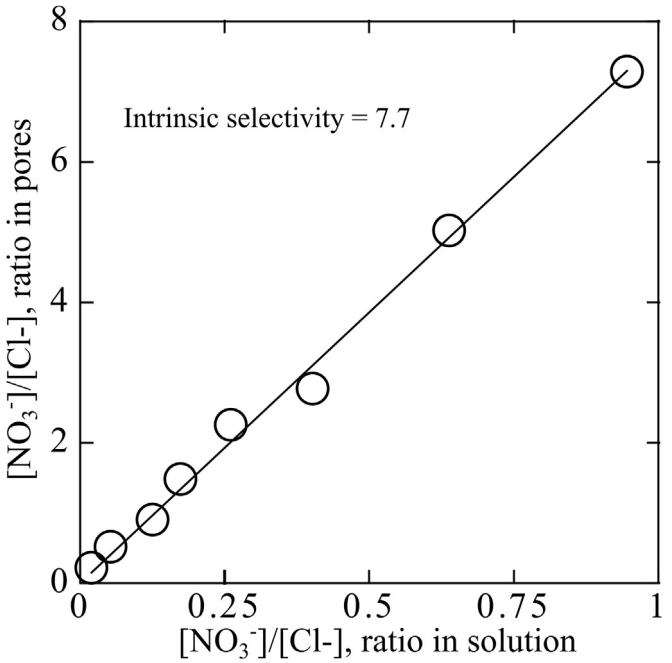

Fig. 2. Controlled, ex-situ experiment to determine intrinsic selectivity of nitrate over chloride. CTA-AC is soaked in high concentration NaCl solution to have a well-known initial condition. The abscissa is the ratio of nitrate to chloride ions in solution. The ordinate is the ratio of nitrate to chloride ions inside the pores.

4.2. Selective ion removal in i-CDI operation

4.2.1. Dynamic ion adsorption

Fig. 3 shows the dynamic model prediction for nitrate and chloride, and measurements at the outlet of our i-CDI cell (discussed in Section 3.2.2) for the case of 0.4, 0.6, 0.8, 1.0, and 1.2 V regeneration and 0 V adsorption with 2 mM $NaNO_3$ and 2 mM NaCl feed solution. Markers are experimental data measured by IC. During regeneration step, a portion of chemically- and electrically-adsorbed chloride and nitrate are expelled from CTA-AC electrode and are flushed from the cell. Similarly, sodium ions are expelled from DBS-AC counter electrode. Also, the regeneration phase for nitrate has longer duration than that of the chloride in order to account for the higher affinity of quaternary ammonium groups towards nitrate. Higher affinity implies a larger number of moles of nitrate in the functional groups. As discussed in our previous work (Oyarzun et al., 2018; Palko et al., 2017), the anionic surfactant on DBS-AC counter electrode provides an electrostatic shield against re-adsorption of nitrate and chloride. We stress that this treatment is thus a critical component of our desalination system.

In the adsorption step (at 0 V), chloride and nitrate are removed from the solution at different rates consistent with mass transport dynamics coupling with the different intrinsic anion selectivity of CTA-AC. At the beginning of adsorption, nitrate and chloride concentration both drop rapidly. At longer times, however, chloride concentration approaches the inlet value noticeably faster than nitrate. Moreover, chloride concentration increases beyond the inlet value shortly after start of adsorption step, while nitrate concentration stays below the inlet value during the adsorption step. This behavior is strong evidence of ion exchange on CTA-AC surface. A similar phenomenon is also observed in adsorption of cations of different valence and hydrated radii (such as Na^+, Mg^{2+}, and Ca^{2+}) in traditional CDI operation (Dykstra et al., 2016; Seo

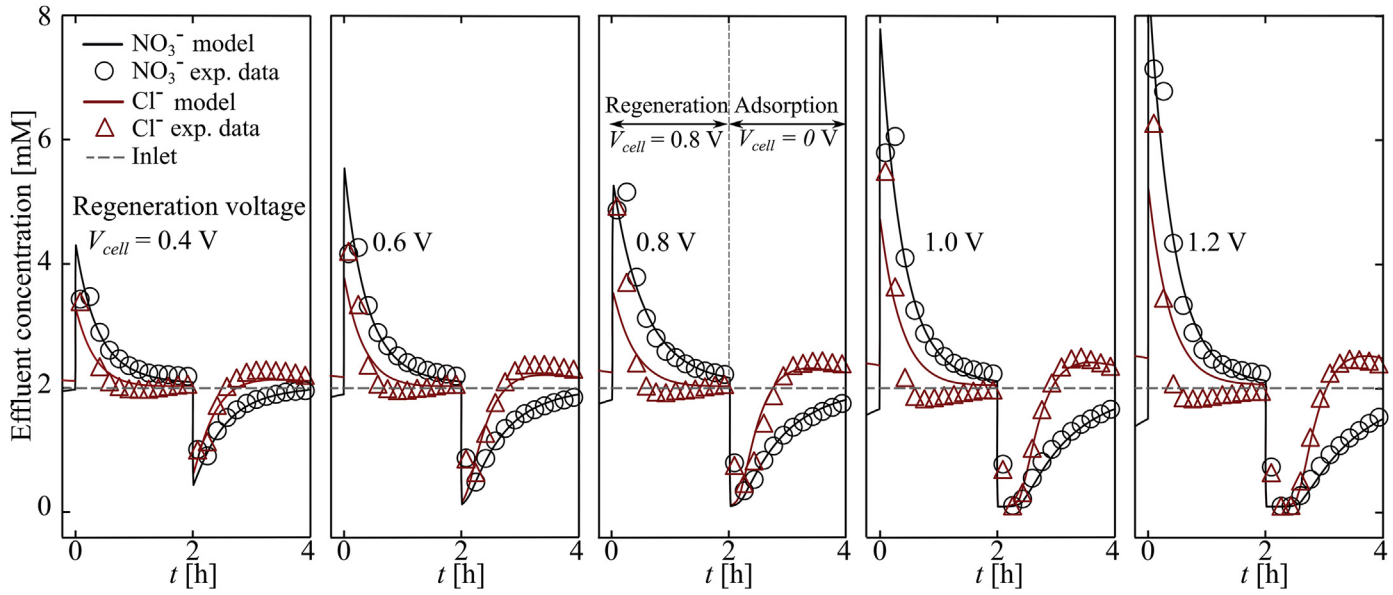

Fig. 3. Cyclic adsorption of nitrate and chloride during electrical regeneration and then passive adsorption. Time series showing independently measured values of NO_3^- and Cl^- concentration versus time in the same effluent stream. Input concentrations is 2 mM$NaNO_3$ and 2 mM NaCl, and constant flow rate Q = 0.43 mL min^{-1}. Shown together with data are predictions from the multi-species model (solid lines). Each cycle is labeled with the applied voltage of the regeneration step. Each measured full cycle (regeneration and adsorption step) correspond to the fourth cycle. First, second, and third cycle were discarded to ensure dynamic steady state.

et al., 2010; Suss, 2017; Zhao et al., 2012).

In Fig. 3, solid lines are the model predictions using $K_{Na} = 10\ \frac{mol}{m^3}$ and $K_{NO_3} = 77\ \frac{mol}{m^3}$ as fitting parameters. K_{Cl} is determined using the measured intrinsic selectivity $k_{int} \approx 7.7$ as $K_{Cl} = K_{NO_3}/k_{int}$ (Eq. (20)). Parameters and other constants used are listed in Table S1 of the SI. The model predictions of selectivity agree well with IC measurements of effluent concentrations, particularly during the adsorption step. The model further captures the ionic exchange between chloride and nitrate ions during adsorption. At higher regeneration voltages the model predictions for effluent chloride dynamics during the regeneration phase deviate somewhat from the respective measurements. We hypothesize that this discrepancy at higher voltages is due to a competition with a third species, hydroxide, which may be generated by Faradaic reactions.

4.2.2. *Effect of regeneration voltage and ratio of concentrations in cycle selectivity*

Fig. 4a and b summarize nitrate and chloride adsorption capacity of our cell (μmol of anions) as a function of respectively regeneration voltage and ratio of feed nitrate concentration over chloride concentration. Nitrate concentration was fixed (2 mM) in all the experiments and chloride concentration varied between 2 and 8 mM. Markers are experimental measurements for each species. Fig. 4c shows cycle selectivity for feed chloride concentration from 2 to 8 mM at fixed (2 mM) feed nitrate concentration and regeneration voltage of 1 V. Cycle selectivity slightly increases with high feed chloride concentration.

Fig. 4d shows cycle selectivity at regeneration voltages from 0.4 to 1.2 V. At 0 V adsorption, cycle selectivity approaches the intrinsic selectivity value as expected. Experiments show cycle selectivity (defined in eq. (24)) decreases with regeneration voltage magnitude. The applied electronic charge, during regeneration, at the carbon surface is sufficient to electrostatically repel both anionic species from the surface with no observable preference, i.e. fraction of desorbed ions is proportional to total moles present on the AC. This implies that the estimated ions released into the stream during regeneration is a strong function of applied voltage and a weak function of the current cell ion concentration. This non-selective desorption mechanism produces available sites proportional to the initial ratio of species on the porous at the beginning of the regeneration step. A higher desorption voltage produces more available sites on the CTA-AC electrode for both nitrate and chloride. However, due to the presence of quaternary ammonium functional groups on the CTA-AC electrode, nitrate is simultaneously re-adsorbed to the CTA-AC electrode. Further, in Fig. 3, we observe a net deficit of chloride at the effluent during the regeneration (concentration bellow the inlet concentration of chloride). This suggests re-adsorption of chloride ions on the DBS-AC counter electrode during the regeneration. Selectivity data shown in Fig. 4d, as discussed in section 3.2.2 corresponds to 2 h charge and 2 h discharge time. According to Fig. 3, for high regeneration voltages cases, exchange of chloride with nitrate is incomplete (nitrate and chloride concentrations are far from baseline at the end of adsorption step). We believe that a longer cycle time will lead to a complete exchange, which in turn, can increase cycle selectivity in those cases.

4.3. *Up-concentration: a high water recovery method for selective ion removal using i-CDI*

High water recovery (WR) is beneficial for water treatment processes. However, WR in CDI applications is usually around 50%. In this section, we present an operation method for CDI/i-CDI to increase WR and simultaneously concentrate the high-affinity ion in a fixed volume of regenerated brine. The method we present here can be used to concentrate rare species. In our approach the brine reservoir volume was chosen to be much smaller than the volume of the electrode. Fig. 5 shows concentration of chloride and nitrate in brine reservoir at the end of first eight cycles. Markers are measured values and lines are least square regressions with $R^2 = 0.97$ for chloride and 0.99 for nitrate. Concentration of ions in the reservoir linearly increases up to respectively 1.7 and 3 mM for chloride and nitrate by the end of last (8th) cycle. This is equivalent to an average increase of about 2.1 mg g^{-1} (37 μmol g^{-1}) NaCl and 5.9 mg g^{-1} (70 μmol g^{-1}) $NaNO_3$ per cycle (based on dry mass of all electrodes). The (molar) cycle selectivity of nitrate with respect to

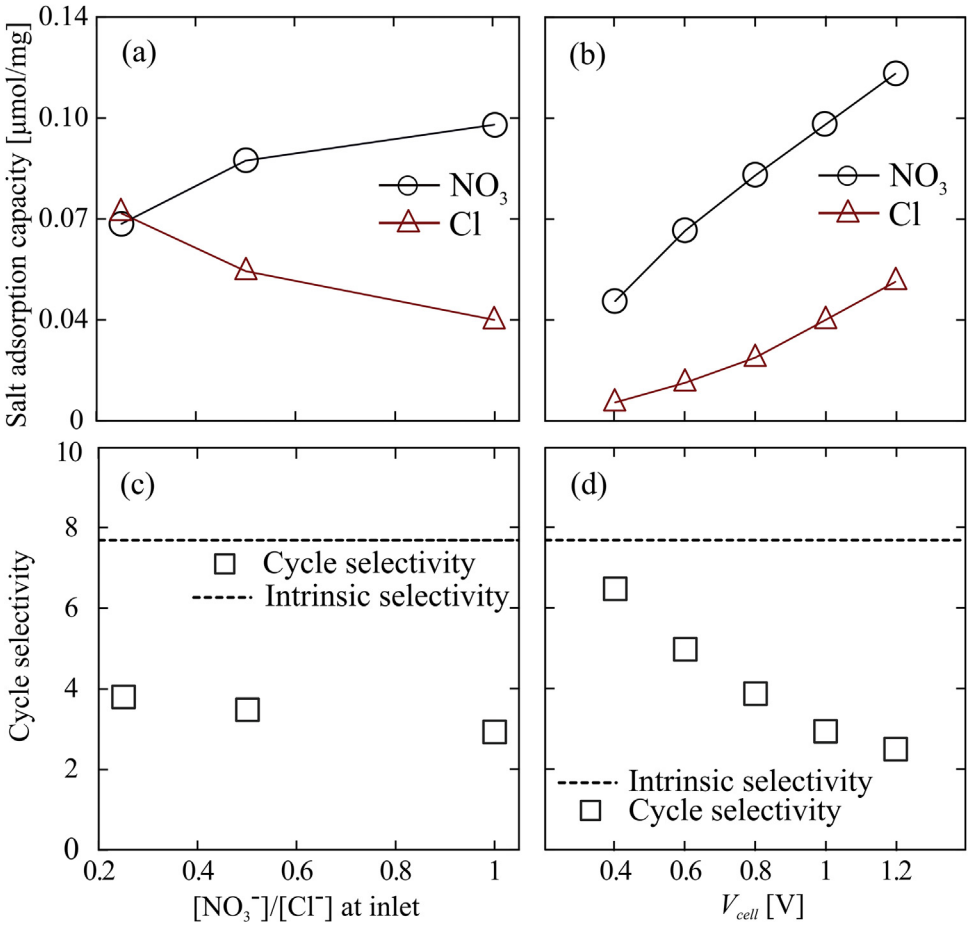

Fig. 4. Cyclic selectivity under various operational modes. a) and c) show salt adsorption capacity for nitrate and chrolide, and cycle selectivity at 2:8, 2:4 and 2:2 ratios of initial concentrations. Nitrate was fixed at 2 mM while chloride was 2, 4 and 8 mM. Regeneration voltages where fixed at 1 V. b) and d) show specific salt adsorption for nitrate and chrolide as well as cycle selectivity at different regeneration voltages. Inlet concentration was constant at 2 mM nitrate and 2 mM chloride. Flow rate was a constant of 0.43 mL min^{-1}.

chloride is thus about 1.9, smaller than 7.7 intrinsic selectivity and even 3.0 cycle selectivity in i-CDI experiment in Section 5.2 (at similar 1 V voltage level). We hypothesize this decline in cycle selectivity, in part, is due to incomplete air flush step (solution is partially removed from tubing and the cell interior). This is particularly true for the smallest pores which have the highest capillary pressure. Moreover, the partially-wet macropores of the electrode after the air flush step have similar nitrate and chloride concentrations. This increase mixing with the brine reservoir solution during the subsequent regeneration step and thus reduces the nitrate selectivity. But nonetheless, Fig. 5 shows successful selective removal of nitrate from feed solution and storage in a brine reservoir. Since we use a fixed brine volume and an open cycle to remove ions, WR increases from 86% at the end of first cycle to 98% at the end of the eighth cycle. We observe a linear relationship up to the eighth cycle; however, we expect a deviation from linear after more cycles due to concentration equilibrium between microporous and brine concentration.

5. Conclusions

We showed a nitrate selective i-CDI system with simple functionalization of electrodes with surfactants. The active electrode was functionalized with CTAB and the counter electrode with SDBS. We first measured the intrinsic selectivity of CTA-AC for nitrate over chloride to be ~7.7 using a controlled ex-situ experiment. We defined cycle selectivity as a parameter which takes into consideration the coupling of electrostatics and mass transport limitations. Our experiments showed that an increase in regeneration voltage magnitude decreases cycle selectivity. In the limiting case, at 0 V, cycle selectivity approaches intrinsic selectivity, as expected. We developed a dynamic model to predict the dynamic steady state of adsorption/regeneration of a i-CDI system with functionalized electrodes. Our model assumes a predominant effect of surface groups over native weak electrolyte surface charge groups on the AC surface. Our model presents good agreement with IC measurements of dynamic steady state for the low affinity (Cl-) and high affinity (NO3-) ion.

We explored a method of increasing water recovery while increasing the concentration of the high-affinity species (here, nitrate) over that of lower affinity species (chloride). To this end, we implemented a novel multi-pass, air-flush i-CDI operation of our functionalized cell design.

We showed nitrate ions are preferentially adsorbed to the positive electrode from the feed solution (during adsorption step). Subsequently, we used an air-flush step to minimize cross-contamination and then desorbed the ions into a small (154 mL) brine reservoir. We showed a successful selective nitrate separation from the feed solution to brine reservoir with cyclic selectivity of about 1.9.

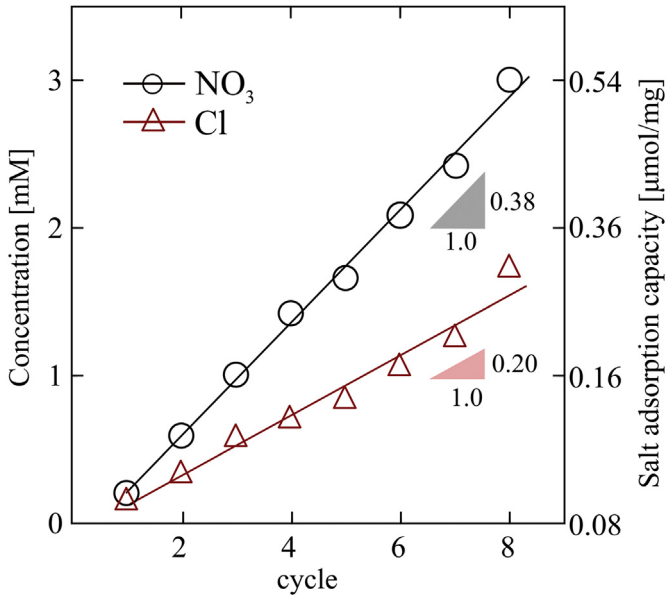

Fig. 5. Nitrate and chloride concentration increment in the regeneration reservoir as a function of number of a completed cycle. Each cycle has an (1) open circuit adsorption, (2) air flush, (3) close loop reservoir desorption, and (4) air flush. Air flush between steps was performed to reduce cross-contamination. Red squares and blue circles are nitrate and chloride concentration, respectively. (For interpretation of the references to colour in this figure legend, the reader is referred to the Web version of this article.)

Declaration of interests

The authors declare that they have no known competing financial interests or personal relationships that could have appeared to influence the work reported in this paper.

Acknowledgments

We gratefully acknowledge funding from TomKat Center for Sustainable Energy at Stanford University. D.I.O would like to thank the support of CONICYT-BECAS CHILE/72160536. A.H. gratefully acknowledges the support from the Stanford Graduate Fellowship program of Stanford University. Work at LLNL was performed under the auspices of the US DOE by LLNL under Contract DE-AC52-07NA27344.

Appendix A. Supplementary data

Supplementary data to this article can be found online at https://doi.org/10.1016/j.wroa.2018.100008.

References

Barron, R.E., Fritz, J.S., 1984. Effect of functional group structure and exchange capacity on the selectivity of anion exchangers for divalent anions. J. Chromatogr. A 316, 201–210. https://doi.org/10.1016/S0021-9673(00)96152-1.

Biesheuvel, P.M., Fu, Y., Bazant, M.Z., 2011. Diffuse charge and Faradaic reactions in porous electrodes. Phys. Rev. E 83, 061507. https://doi.org/10.1103/PhysRevE.83.061507.

Biesheuvel, P.M., Suss, M.E., Hamelers, H.V.M., 2015. Theory of Water Desalination by Porous Electrodes with Fixed Chemical Charge. arXiv:1506.03948 [cond-mat, physics:physics] 9, 1–10. https://doi.org/10.1016/j.colcom.2015.12.001

Bouchard, D.C., Williams, M.K., Surampalli, R.Y., 1992. Nitrate contamination of groundwater: sources and potential health effects. J./Am. Water Work. Assoc. 84, 85–90. https://doi.org/10.1002/j.1551-8833.1992.tb07430.x.

Chekli, L., Phuntsho, S., Kim, J.E., Kim, J., Choi, J.Y., Choi, J.S., Kim, S., Kim, J.H., Hong, S., Sohn, J., Shon, H.K., 2016. A comprehensive review of hybrid forward osmosis systems: performance, applications and future prospects. J. Membr. Sci. https://doi.org/10.1016/j.memsci.2015.09.041.

Dykstra, J.E., Dijkstra, J., van der Wal, A., Hamelers, H.V.M., Porada, S., 2016. On-line method to study dynamics of ion adsorption from mixtures of salts in capacitive deionization. Desalination 390, 47–52. https://doi.org/10.1016/j.desal.2016.04.001.

Dykstra, J.E., Keesman, K.J., Biesheuvel, P.M., van der Wal, A., 2017. Theory of pH changes in water desalination by capacitive deionization. Water Res. 119, 178–186. https://doi.org/10.1016/j.watres.2017.04.039.

Farmer, J.C., Fix, D.V., Mack, G.V., Pekala, R.W., Poco, J.F., 1996. Capacitive deionization of NH4ClO4 solutions with carbon aerogel electrodes. J. Appl. Electrochem. 26, 1007–1018. https://doi.org/10.1007/BF00242195.

Gao, X., Omosebi, A., Landon, J., Liu, K., 2015. Enhanced salt removal in an inverted capacitive deionization cell using amine modified microporous carbon cathodes. Environ. Sci. Technol. 49, 10920–10926. https://doi.org/10.1021/acs.est.5b02320.

Ghaemi, N., Daraei, P., Akhlaghi, F.S., 2018. Polyethersulfone nanofiltration membrane embedded by chitosan nanoparticles: fabrication, characterization and performance in nitrate removal from water. Carbohydr. Polym. 191, 142–151. https://doi.org/10.1016/j.carbpol.2018.03.024.

Han, L., Karthikeyan, K.G., Anderson, M.A., Gregory, K.B., 2014. Exploring the impact of pore size distribution on the performance of carbon electrodes for capacitive deionization. J. Colloid Interface Sci. 430, 93–99. https://doi.org/10.1016/j.jcis.2014.05.015.

Harland, C.E. (Ed.), 1994. Ion exchange equilibria, in: Ion Exchange: Theory and Practice. The Royal Society of Chemistry, pp. 90–133. https://doi.org/10.1039/9781847551184-00090

Hasnat, A., Juvekar, V.A., 1996. Ion-exchange kinetics: heterogeneous resin-phase model. AIChE J. 42, 161–175. https://doi.org/10.1002/aic.690420114.

He, F., Biesheuvel, P.M., Bazant, M.Z., Hatton, T.A., 2018. Theory of water treatment by capacitive deionization with redox active porous electrodes. Water Res. 132, 282–291. https://doi.org/10.1016/j.watres.2017.12.073.

Helfferich, F.G., 1962. Ion Exchange. Courier Corporation.

Hemmatifar, A., Oyarzun, D.I., Palko, J.W., Hawks, S.A., Stadermann, M., Santiago, J.G., 2017. Equilibria model for pH variations and ion adsorption in capacitive deionization electrodes. Water Res. https://doi.org/10.1016/j.watres.2017.05.036.

Hemmatifar, A., Stadermann, M., Santiago, J.G., 2015. Two-dimensional porous electrode model for capacitive deionization. J. Phys. Chem. C 119, 24681–24694. https://doi.org/10.1021/acs.jpcc.5b05847.

Hou, C.H., Huang, C.Y., 2013. A comparative study of electrosorption selectivity of ions by activated carbon electrodes in capacitive deionization. Desalination 314, 124–129. https://doi.org/10.1016/j.desal.2012.12.029.

Hou, C.H., Taboada-Serrano, P., Yiacoumi, S., Tsouris, C., 2008. Electrosorption selectivity of ions from mixtures of electrolytes inside nanopores. J. Chem. Phys. 129. https://doi.org/10.1063/1.3033562.

Inoue-Choi, M., Jones, R.R., Anderson, K.E., Cantor, K.P., Cerhan, J.R., Krasner, S., Robien, K., Weyer, P.J., Ward, M.H., 2014. Nitrate and nitrite ingestion and risk of ovarian cancer among postmenopausal women in Iowa. Int. J. Canc. 00, 1–10. https://doi.org/10.1002/ijc.29365.

Jamaly, S., Darwish, N.N., Ahmed, I., Hasan, S.W., 2014. A short review on reverse osmosis pretreatment technologies. Desalination. https://doi.org/10.1016/j.desal.2014.09.017.

Jones, R.R., Weyer, P.J., Dellavalle, C.T., Inoue-Choi, M., Anderson, K.E., Cantor, K.P., Krasner, S., Robien, K., Beane Freeman, L.E., Silverman, D.T., Ward, M.H., 2016. Nitrate from drinking water and diet and bladder cancer among postmenopausal women in Iowa. Environ. Health Perspect. 124, 1751–1758. https://doi.org/10.1289/EHP191.

Kim, Y.J., Choi, J.H., 2012. Selective removal of nitrate ion using a novel composite carbon electrode in capacitive deionization. Water Res. 46, 6033–6039.

Kim, Y.J., Kim, J.H., Choi, J.H., 2013. Selective removal of nitrate ions by controlling the applied current in membrane capacitive deionization (MCDI). J. Membr. Sci. https://doi.org/10.1016/j.memsci.2012.11.064.

Kumar, R., Pal, P., 2015. A novel forward osmosis-nano filtration integrated system for coke-oven wastewater reclamation. Chem. Eng. Res. Des. 100, 542–553. https://doi.org/10.1016/j.cherd.2015.05.012.

Lado, J.J., Pérez-Roa, R.E., Wouters, J.J., Tejedor-Tejedor, M.I., Federspill, C., Ortiz, J.M., Anderson, M.A., 2017. Removal of nitrate by asymmetric capacitive deionization. Separ. Purif. Technol. 183, 145–152. https://doi.org/10.1016/j.seppur.2017.03.071.

Lee, D.H., Ryu, T., Shin, J., Ryu, J.C., Chung, K.S., Kim, Y.H., 2017. Selective lithium recovery from aqueous solution using a modified membrane capacitive deionization system. Hydrometallurgy 173, 283–288. https://doi.org/10.1016/j.hydromet.2017.09.005.

Li, Y., Zhang, C., Jiang, Y., Wang, T.J., Wang, H., 2016. Effects of the hydration ratio on the electrosorption selectivity of ions during capacitive deionization. Desalination 399, 171–177. https://doi.org/10.1016/j.desal.2016.09.011.

Mubita, T.M., Porada, S., Biesheuvel, P.M., van der Wal, A., Dykstra, J.E., 2018. Capacitive deionization with wire-shaped electrodes. Electrochim. Acta 270, 165–173. https://doi.org/10.1016/j.electacta.2018.03.082.

Nie, C., Zhan, Y., Pan, L., Li, H., Sun, Z., 2011. Electrosorption of different cations and anions with membrane capacitive deionization based on carbon nanotube/nanofiber electrodes and ion-exchange membranes. Desalin. Water Treat. 30, 266–271. https://doi.org/10.5004/dwt.2011.2089.

Oren, Y., 2008. Capacitive deionization (CDI) for desalination and water treatment - past, present and future (a review). Desalination 228, 10–29. https://doi.org/10.1016/j.desal.2007.08.005.

Oyarzun, D.I., Hemmatifar, A., Palko, J.W., Stadermann, M., Santiago, J.G., 2018. Adsorption and capacitive regeneration of nitrate using inverted capacitive

deionization with surfactant functionalized carbon electrodes. Separ. Purif. Technol. 194, 410–415. https://doi.org/10.1016/j.seppur.2017.11.027.
Palko, J.W., Oyarzun, D.I., Ha, B., Stadermann, M., Santiago, J.G., 2017. Nitrate removal from water using electrostatic regeneration of functionalized adsorbent. Chem. Eng. J. https://doi.org/10.1016/j.cej.2017.10.161.
Persat, A., Suss, M.E., Santiago, J.G., 2009. Basic principles of electrolyte chemistry for microfluidic electrokinetics. Part II: coupling between ion mobility, electrolysis, and acid-base equilibria. Lab a Chip 9, 2454–2469. https://doi.org/10.1039/b906468k.
Richards, L.A., Richards, B.S., Schäfer, A.I., 2011. Renewable energy powered membrane technology: salt and inorganic contaminant removal by nanofiltration/reverse osmosis. J. Membr. Sci. 369, 188–195. https://doi.org/10.1016/j.memsci.2010.11.069.
Samatya, S., Kabay, N., Yüksel, Ü., Arda, M., Yüksel, M., 2006. Removal of nitrate from aqueous solution by nitrate selective ion exchange resins. React. Funct. Polym. 66, 1206–1214. https://doi.org/10.1016/j.reactfunctpolym.2006.03.009.
Seo, S.J., Jeon, H., Lee, J.K., Kim, G.Y., Park, D., Nojima, H., Lee, J., Moon, S.H., 2010. Investigation on removal of hardness ions by capacitive deionization (CDI) for water softening applications. Water Res. 44, 2267–2275. https://doi.org/10.1016/j.watres.2009.10.020.
Siekierka, A., Bryjak, M., 2017. Hybrid capacitive deionization with anion-exchange membranes for lithium extraction. E3S Web Conf. 22, 00157. https://doi.org/10.1051/e3sconf/20172200157.
Siekierka, A., Bryjak, M., Wolska, J., 2017a. The use of activated carbon modified with polypyrrole as a supporting electrode for lithium ions adsorption in capacitive deionization. Desalin. Water Treat. 64, 251–254. https://doi.org/10.5004/dwt.2017.11387.
Siekierka, A., Wolska, J., Bryjak, M., Kujawski, W., 2017b. Anion exchange membranes in lithium extraction by means of capacitive deionization system. Desalin. Water Treat. 75, 331–341. https://doi.org/10.5004/dwt.2017.20431.
Subramani, A., Jacangelo, J.G., 2015. Emerging desalination technologies for water treatment: a critical review. Water Res. https://doi.org/10.1016/j.watres.2015.02.032.
Suss, M.E., 2017. Size-based ion selectivity of micropore electric double layers in capacitive deionization electrodes. J. Electrochem. Soc. 164, E270–E275. https://doi.org/10.1149/2.1201709jes.
Tang, W., Kovalsky, P., Cao, B., He, D., Waite, T.D., 2016a. Fluoride removal from brackish groundwaters by constant current capacitive deionization (CDI). Environ. Sci. Technol. 50, 10570–10579. https://doi.org/10.1021/acs.est.6b03307.
Tang, W., Kovalsky, P., Cao, B., Waite, T.D., 2016b. Investigation of fluoride removal from low-salinity groundwater by single-pass constant-voltage capacitive deionization. Water Res. 88, 112–121. https://doi.org/10.1016/j.watres.2016.04.047.
Tang, W., Kovalsky, P., He, D., Waite, T.D., 2015. Fluoride and nitrate removal from brackish groundwaters by batch-mode capacitive deionization. Water Res. 84, 342–349. https://doi.org/10.1016/j.watres.2015.08.012.
Werber, J.R., Deshmukh, A., Elimelech, M., 2016. The critical need for increased selectivity, not increased water permeability, for desalination membranes. Environ. Sci. Technol. Lett. 3, 112–120. https://doi.org/10.1021/acs.estlett.6b00050.
Wheaton, R.M., Bauman, W.C., 1951. Properties of strongly basic anion exchange resins. Ind. Eng. Chem. 43, 1088–1093. https://doi.org/10.1021/ie50497a027.
World Health Organization, 2011. Nitrate and nitrite in drinking-water. Backgr. Doc. Dev. WHO Guidel. Drink. Qual. 37, 227–231. https://doi.org/10.1159/000225441.
Xie, M., Nghiem, L.D., Price, W.E., Elimelech, M., 2012. Comparison of the removal of hydrophobic trace organic contaminants by forward osmosis and reverse osmosis. Water Res. 46, 2683–2692. https://doi.org/10.1016/j.watres.2012.02.023.
Xu, X., Gao, B., Zhao, Y., Chen, S., Tan, X., Yue, Q., Lin, J., Wang, Y., 2012. Nitrate removal from aqueous solution by Arundo donax L. reed based anion exchange resin. J. Hazard. Mater. 203–204, 86–92. https://doi.org/10.1016/j.jhazmat.2011.11.094.
Yeo, J.-H., Choi, J.-H., 2013. Enhancement of nitrate removal from a solution of mixed nitrate, chloride and sulfate ions using a nitrate-selective carbon electrode. Desalination 320, 10–16. https://doi.org/10.1016/j.desal.2013.04.013.
Zhao, R., van Soestbergen, M., Rijnaarts, H.H.M., van der Wal, A., Bazant, M.Z., Biesheuvel, P.M., 2012. Time-dependent ion selectivity in capacitive charging of porous electrodes. J. Colloid Interface Sci. 384, 38–44. https://doi.org/10.1016/j.jcis.2012.06.022.
Zhao, Y., Zhang, Z., Dai, L., Mao, H., Zhang, S., 2017. Enhanced both water flux and salt rejection of reverse osmosis membrane through combining isophthaloyl dichloride with biphenyl tetraacyl chloride as organic phase monomer for seawater desalination. J. Membr. Sci. 522, 175–182. https://doi.org/10.1016/j.memsci.2016.09.022.